euronoise

Influence of material properties on sound radiation for flat loudspeakers

Jaime Ramis Soriano[a], Jesús Alba Fernandez[b], Jorge Frances Monllor[a] and Jorge P. Arenas Bermudez[c]

[a]DFISTS. Univ. de Alicante, Carretera de Sant Vicent del Raspeig s/n, 03690 San Vicente del Raspeig, Spain
[b]Escola Politècnica Superior de Gandia, Universitat Politècnica de València, Crtra Natzaret-Oliva s/n, 46730 Gandia, Spain
[c]Universidad Austral de Chile, Institute of Acoustics, 567 Valdivia, Chile
jramis@ua.es

This work aims to study the influence of some material properties on the sound radiation characteristics of a flat loudspeaker using numerical, analytical, and experimental procedures. A shaker, whose mechanical characteristics are completely known, is used here as the excitation force for the experimental study. Finite Element Method has been used to simulate this configuration. An analytical model that couples the electrical, mechanical and acoustical system of the panel has been used for comparison. Influence of the elastic modulus and damping loss factor of the panel materials are the main subject of this research. The analytical formulation provides the basis for studying the structural and vibrational behavior of the system. The results obtained for different materials and different excitation locations may be used for optimizing this type of loudspeakers.

1 Introduction

In general, the basic structure of a panel loudspeaker consists of a plate and one or several inertia exciters (see Fig. 1). The main advantages of a panel loudspeaker as compared with conventional ones are its compactness and low directivity.

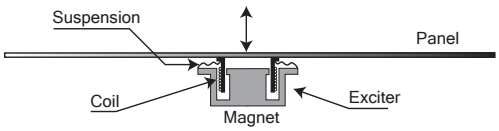

Figure 1: Panel loudspeaker with an exciter attached.

Several studies have used electro-mechanical analogies for modeling vibration exciters [2, 3]. Figure 2 shows the equivalent circuit of the total system using a mobility analogy.

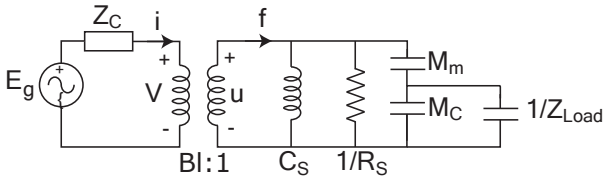

Figure 2: Electro-mechanical analogy of a panel loudspeaker (mobility).

Although oversimplified, the analysis of equivalent circuits provides a useful tool for predicting the behavior of a loudspeaker. However, this work is focused on the influence of the Young's modulus on sound power and directivity. Then, instead of the inertia exciter used in conventional panel loudspeakers, a shaker having well-known properties is employed here to use the maximum information in the algorithm. The shaker is an essential piece of test equipment for vibration-proof testing of electronic products. The estimation based on measurements for obtaining accurate model parameters is necessary, and it has been discussed in [4].

2 Experimental set-up

Let us consider a panel of dimensions 31.4 cm × 42 cm, which is divided into 108 elements, as shown in Fig. 3. The shaker is fixed at two different positions labeled as A and B.

A modal exciter UA-4824 from B&K attached to a support specifically designed for the panel size was used for the measurements. Figure 4 shows the experimental

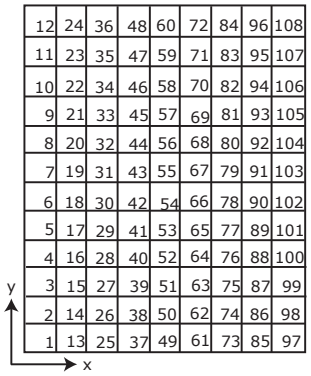

Figure 3: Mesh of 108 elements used to discretize the panel.

set-up placed inside an anechoic chamber of the University of Alicante.

Different core panel materials were considered and their Young's modulus were measured using a B&K impact hammer and a B&K accelerometer, according to the method described by ASTM [8]. In this method, Young's modulus is measured in a single beam sample vibrating in several of its modes, so the material properties are determined as a function of frequency. In these tests, measurements were made using the base beam damped on one side. The experimental set-up is shown in Fig. 5.

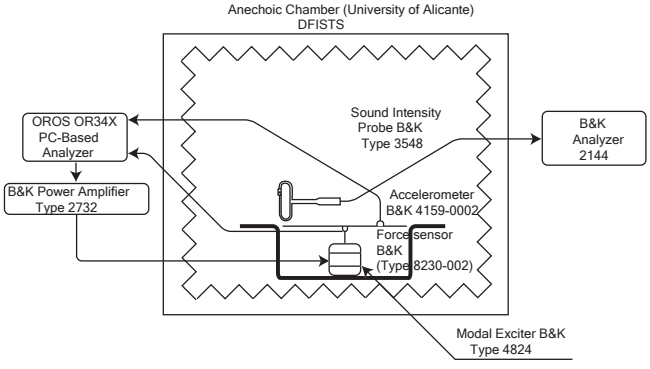

Figure 4: Acceleration and sound intensity measures in the anechoic chamber.

3 Theory

In this section, details of the measurement model of the panel-exciter system are given. Measures of Young's modulus of the materials and shaker analysis are shown. Two sample beams of the material used to made the

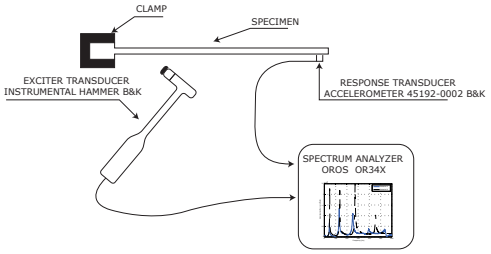

Figure 5: Experimental set-up using a two-channel spectrum analyzer and B&K modal Hammer.

flat loudspeaker are tested using the ASTM method and then simulated using the Euler-Bernoulli model [1].

3.1 Influence of Young's modulus on mechanical impedance ($\mathbf{Z_m}$)

Assuming light fluid loading, the relationship between the concentrated force vector $\mathbf{f}$ and the velocity vector $\mathbf{v}$ can be written as

$$\mathbf{f} = \mathbf{Z_m}\mathbf{v}. \tag{1}$$

The assumed-modes method is employed to evaluate the mechanical impedance matrix $\mathbf{Z_m}$ [5, 7]. For a simply-supported plate of dimensions $L_y \times L_y$ and material constants D and μ, the resonance frequencies are

$$\omega_{mn} = \sqrt{\frac{D}{\mu}}\Big[(m\pi/L_x)^2 + (n\pi/L_y)^2\Big], \tag{2}$$

where m and n are integers. The normalized eigenfunctions of the panel are

$$\phi_{mn}(x,y) = \frac{2}{\sqrt{L_x L_y}} \sin(m\pi x/L_x)\sin(n\pi y/L_y). \tag{3}$$

We can express the displacement of the plate as

$$w(x,y,t) = \sum_{i=1}^{l} \phi_i(x,y) q_i(t), \tag{4}$$

where l is the total number of modes considered and $q_i(t)$ is the generalized coordinate. The admissible functions can be found by either analytical or numerical methods such as the finite-element method.

The strain energy of the plate is

$$\begin{aligned} U =& \frac{D}{2}\int_0^{L_x}\int_0^{L_y} \Big[w_{xx}^2(x,y,t) + w_{yy}^2(x,y,t) \\ &+ 2v w_{xx}(x,y,t) w_{yy}(x,y,t) \\ &+ 2(1-v) w_{xy}^2(x,y,t)\Big] dxdy, \end{aligned} \tag{5}$$

where

$$D = \frac{Eh^3}{12(1-v^2)} \tag{6}$$

is the bending stiffness of the plate, E is the Young's modulus, v is the Poisson ratio, and h is the thickness of the panel. The subscripts of w indicate differentiation of w with respect to that subscript. Now, the kinetic energy is given by

$$T = \frac{1}{2}\int_0^{L_x}\int_0^{Ly} \mu w_t^2(x,y,t) dxdy, \tag{7}$$

where μ is the surface mass density. The virtual work done by the exciting force $f(x,y,t)$ is

$$\delta W = \int_0^{L_x}\int_0^{L_y} f(x,y,t)\delta w(x,y,t) dxdy. \tag{8}$$

Using the assumed-modes method, we can rewrite Eqs. (5), (7), and (8) as

$$U = \frac{1}{2}\sum_{i=1}^{l}\sum_{j=1}^{l} k_{ij} q_i(t) q_j(t), \tag{9}$$

where k_{ij} are the elements of the modal stiffness matrix,

$$\begin{aligned} k_{ij} =& D\int_0^{L_x}\int_0^{L_y} \Big[\phi_{i,xx}(x,y)\phi_{j,xx}(x,y) \\ &+ \phi_{i,yy}(x,y)\phi_{i,yy}(x,y) \\ &+ 2v\phi_{i,xx}(x,y)\phi_{i,yy}(x,y) \\ &+ 2(1-v)\phi_{i,xy}(x,y)\phi_{i,xy}(x,y)\Big] dxdy, \end{aligned} \tag{10}$$

$$T = \frac{1}{2}\sum_{i=1}^{l}\sum_{j=1}^{l} m_{ij}\dot{q}_i(t)\dot{q}_j(t), \tag{11}$$

where m_{ij} are the elements of the modal mass matrix,

$$m_{ij} = \mu\int_0^{L_x}\int_0^{L_y} \phi_i(x,y)\phi_j(x,y) dxdy, \tag{12}$$

$$\delta W = \sum_{i=1}^{l} f_i \delta q_i(t), \tag{13}$$

where

$$f_i = \mu\int_0^{L_x}\int_0^{L_y} f(x,y,t)\phi_i(x,y) dxdy. \tag{14}$$

Defining the Lagrangian $L = T - U$, it follows that

$$\frac{\partial}{\partial t}\left(\frac{\partial L}{\partial \dot{q}_i}\right) - \frac{\partial L}{\partial q_i} = f_i \quad i = 1, \cdots, l \tag{15}$$

Substituting Eqs. (9), (11) and (13) into Eq. (15) leads to the following matrix differential equation

$$\hat{\mathbf{M}}\ddot{\mathbf{q}} + \hat{\mathbf{K}}\mathbf{q} = \mathbf{f}, \tag{16}$$

where $\hat{\mathbf{M}}$ and $\hat{\mathbf{K}}$ are the modal mass matrix and the modal stiffness matrix, respectively. Then, from Eq. (16), we can identify the modal mechanical impedance matrix of the panel

$$\hat{\mathbf{Z}}_\mathbf{m} = \frac{\hat{\mathbf{K}} - \omega^2\hat{\mathbf{M}}}{j\omega}. \tag{17}$$

We can see from Eq. (10) that the Young's modulus is directly associated with the parameters involved in the dynamic behavior of our system. On the other hand, it is well-known that determination of changes in the vibration distribution on the surface of the panel gives us an idea of changes in sound power and sound radiation patterns.

3.2 Transverse or bending vibrations

Consider a flexural vibration experiment on a uniform beam composed of a linear, homogeneous, and isotropic viscoelastic material without axial loads, as shown in Fig. 6.

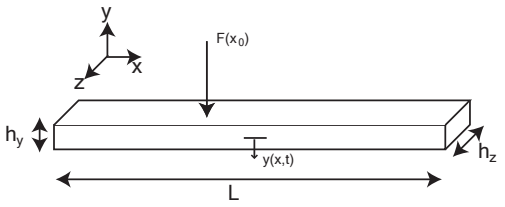

Figure 6: Flexural (transverse or bending) vibration experiment on a beam with length L. $F(x_0)$ is the amplitude of the harmonic applied force and $y(x,t)$ is the transverse displacement as a function of the position x.

According to the Euler-Bernoulli model, the transfer function $G_y(j\omega, x, x_0)$ from the force $F(t)$ at position x_0 to the transverse displacement $y(x,t)$ at position x, is given by

$$G_y^{Euler}(j\omega,x,x_0) = \begin{cases} \frac{B(j\omega,x,x_0)}{A(j\omega)} & \text{if } x \le x_0, \\ \frac{B(j\omega,L-x,L-x_0)}{A(j\omega)} & \text{if } x \ge x_0, \end{cases} \tag{18}$$

where

$$\begin{aligned} B(j\omega,x,x_0) =& K_1(j\omega,x_0)\cos(b(j\omega)x) \\ &+ K_2(s,x_0)\sin(b(j\omega)x) \\ &+ K_3(j\omega,x_0)e^{b(j\omega)x} \\ &+ K_4(j\omega,x_0)e^{-b(j\omega)x}, \end{aligned} \tag{19}$$

and

$$\begin{aligned} A(j\omega) =& 8E(j\omega)Ib^3(s) \\ &\times (\cosh(b(j\omega)L)\cos(b(j\omega)L) - 1), \end{aligned} \tag{20}$$

where L is the length of the beam, $E(j\omega)$ is the Young's modulus, I the moment of inertia of the cross-section of the beam about the z-axis and $b(j\omega)$ is related to the material properties as

$$\begin{aligned} b(j\omega) &= \sqrt{4}|a(j\omega)|e^{j\frac{\angle a(j\omega)}{4}}, \\ \text{where } a(j\omega) &= -\tfrac{\rho A(j\omega)^2}{E(j\omega)I}, \end{aligned} \tag{21}$$

ρ is the density of the material, and A is the cross-section area ($A = h_z h_y$ for a rectangle with sides h_z and h_y). The functions $K_i(j\omega, x_0)$ are given by

$$\begin{aligned} \frac{K_1(j\omega,x_0)}{2} =& -\sin(b(j\omega)x_0) + \sin(b(j\omega)x_0) \\ &- \sinh(b(j\omega)(L-x_0))\cos(b(j\omega)L) \\ &+ \cosh(b(j\omega)(L-x_0))\sin(b(j\omega)L) \\ &+ \cos(b(j\omega)L)\sin(b(j\omega)(L-x_0)) \\ &- \sinh(b(j\omega)L)\cos(b(j\omega)(L-x_0)), \end{aligned} \tag{22}$$

$$\begin{aligned} \frac{K_2(j\omega,x_0)}{2} =& \cosh(b(j\omega)x_0) - \cos(b(j\omega)x_0) \\ &- \cosh(b(j\omega)(L-x_0))\cos(b(j\omega)L) \\ &- \sinh(b(j\omega)(L-x_0))\sin(b(j\omega)L) \\ &+ \cosh(b(j\omega)L)\cos(b(j\omega)(L-x_0)) \\ &- \sinh(b(j\omega)L)\sin(b(j\omega)(L-x_0)), \end{aligned} \tag{23}$$

$$\begin{aligned} \frac{K_3(j\omega,x_0)}{2} =& e^{-b(j\omega)x_0} + \sin(b(j\omega)x_0) \\ &- \cos(b(j\omega)x_0) \\ &+ e^{-b(j\omega)L}(\sin(b(j\omega)(L-x_0)) \\ &+ \cos(b(j\omega)(L-x_0)) \\ &+ \sin(b(j\omega)L)e^{-b(j\omega)(L-x_0)} \\ &- \cos(b(j\omega)L)e^{b(j\omega)(L-x_0)}, \end{aligned} \tag{24}$$

and

$$\begin{aligned} \frac{K_4(j\omega,x_0)}{2} =& -e^{-b(j\omega)x_0} + \sin(b(j\omega)x_0) \\ &+ \cos(b(j\omega)x_0) \\ &+ e^{b(j\omega)L}(\sin(b(j\omega)(L-x_0)) \\ &- \cos(b(j\omega)(L-x_0)) \\ &+ \sin(b(j\omega)L)e^{-b(j\omega)(L-x_0)} \\ &+ \cos(b(j\omega)L)e^{-b(j\omega)(L-x_0)}. \end{aligned} \tag{25}$$

The resonances of the frequency response function $G_y^{Euler}(j\omega, x, x_0)$ are determined by the zeroes $j\omega = jw_k$ of $g^{Euler}(s) = 0$ with

$$g^{Euler}(j\omega) = \cosh(b(j\omega)L)\cos(b(j\omega)L) - 1. \tag{26}$$

Hence, the poles are calculated as

$$g^{Euler}(j\omega_k) = 0 \rightarrow b(j\omega_k)L = \xi_k, \tag{27}$$

with $k = \pm1, \pm2, \cdots$, and ξ_k is the wave number of the kth resonance frequency [6]. Numerical values of ξ_k are shown in Table 6.4 of reference [6]. Loss factor can be calculated from

$$\eta = \frac{\Delta f_n}{f_n}. \tag{28}$$

Using Eq. (21), the equation for the poles (26) can be rewritten as

$$E(j\omega_k) = -\frac{\rho A L^4 \omega_k^4}{I\xi_k^4} \quad \text{with } k = \pm1, \pm2, \cdots. \tag{29}$$

The Euler-Bernoulli theory that leads to the transfer function given by Eq. (18) and with poles satisfying Eq. (29), ignores the effects of shear deformation and rotary inertia, and is accurate for thin beams. By calculating the Young's modulus from modal response measurements we will see that the theoretical model is in good agreement with the Euler-Bernoulli theory.

3.3 Radiation impedance matrix ($\mathbf{Z_a}$)

If $\mathbf{f_a}$ are the equivalent concentrated forces acting on each element due to acoustic pressure, then the following relation holds

$$\mathbf{f_a} = \mathbf{Z_a}\mathbf{v}. \tag{30}$$

Many methods are available for calculating $\mathbf{Z_a}$. A simple formula is used here to obtain the matrix $\mathbf{Z_a}$ [2]

$$\mathbf{Z_a} = S\rho c \begin{pmatrix} 1 - e^{-jk\sqrt{S/\pi}} & \cdots & \frac{jkS}{2\pi}\frac{e^{-jkr_{1N}}}{r_{1N}} \\ \frac{jkS}{2\pi}\frac{e^{-jkr_{21}}}{r_{21}} & \cdots & \vdots \\ \vdots & \ddots & \vdots \\ \frac{jkS}{2\pi}\frac{e^{-jkr_{N1}}}{r_{N1}} & \cdots & 1 - e^{-jk\sqrt{S/\pi}} \end{pmatrix}, \tag{31}$$

where S is the area of each element, r_{mn} is the distance from the center of the element n to the point m $(m, n = 1, \cdots, N)$.

3.4 Evaluation of the sound pressure and the sound power

The far field sound pressure can be calculated using the linear transformation

$$\mathbf{p} = \mathbf{E}\mathbf{v}, \tag{32}$$

where $\mathbf{p}$ is the far field sound pressure vector, $\mathbf{v}$ is the vector of surface velocity of the panel, and $\mathbf{E}$ is a propagation matrix, which can be calculated as

$$\mathbf{E} = j\frac{\rho_0 ckS}{2\pi} \begin{pmatrix} \frac{e^{-jkr_{11}}}{r_{11}} & \cdots & \frac{e^{-jkr_{1N}}}{r_{1N}} \\ \frac{e^{-jkr_{21}}}{r_{21}} & \cdots & \frac{e^{-jkr_{N}}}{r_{2N}} \\ \vdots & \ddots & \vdots \\ \frac{e^{-jkr_{N1}}}{r_{N1}} & \cdots & \frac{e^{-jkr_{NN}}}{r_{NN}} \end{pmatrix} \tag{33}$$

where r_{mn} is the distance from the center of the element n to the field point m $(m, n = 1, \cdots, M)$.

The radiated sound power can be calculated as

$$\mathbf{W} = \mathbf{v^H}\mathbf{R}\mathbf{v}, \tag{34}$$

where $\mathbf{R} = Re\{\mathbf{Z_a}\}/2$, and the radiation resistance matrix $\mathbf{R}$ is a positive definite matrix given by

$$\mathbf{R} = \frac{\omega^2\rho S^2}{4\pi c} \begin{pmatrix} 1 & \frac{\sin kr_{12}}{kr_{12}} & \cdots & \frac{\sin kr_{1N}}{kr_{1N}} \\ \frac{\sin kr_{21}}{kr_{21}} & 1 & \cdots & \vdots \\ \vdots & \vdots & \ddots & \vdots \\ \frac{\sin kr_{N2}}{kr_{N2}} & \cdots & \cdots & 1 \end{pmatrix}. \tag{35}$$

4 Experimental results

4.1 Young's modulus determination

The force-to-acceleration transfer functions $(s^2 G_z(j\omega))$ measured for both materials are presented in Fig. (7).

Young's modulus and damping loss factor for both panel loudspeaker materials were estimated by Eq. (29) and reference [8]. Figure 8 and Table 4.1 show the values estimated.

Using the experimental data, the modal response is calculated by the analytical model explained in section 3.2. The correlation between the curves allows us to confirm that the frequencies used for calculating the modulus are due solely to the longitudinal bending. The analytical and measured modal curves are compared in Fig. 9. Good agreement is observed which assure that the values obtained are fine enough.

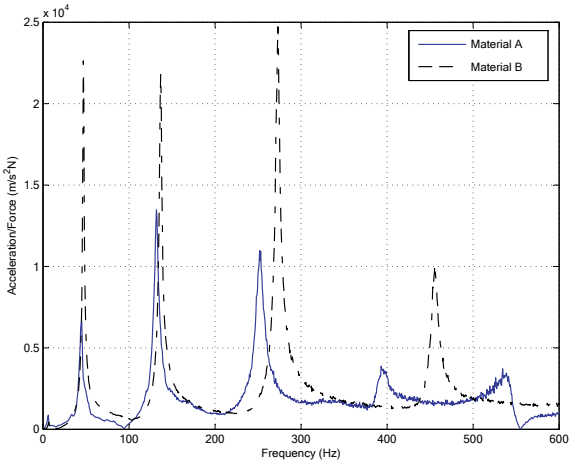

Figure 7: Force-to-acceleration transfer function $s^2 G_y(j\omega)$ of the flexural vibration experiment using materials A and B.

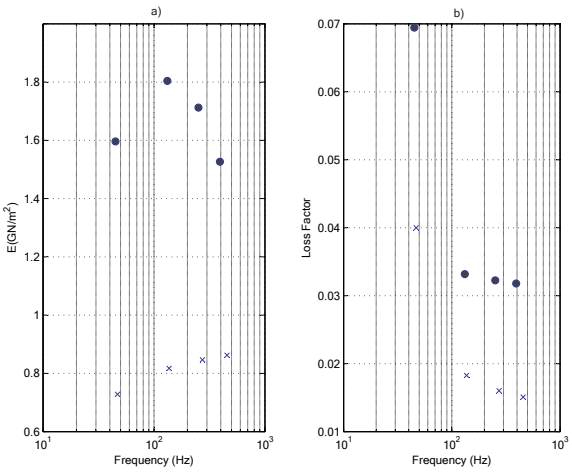

Figure 8: a) Young's modulus versus frequency for A (dots) and B (cross) type material. b) Material damping loss factor versus frequency for A (dots) and B (cross) type material.

4.2 Sound power level and directivity

This section reports the results attained by introducing the acceleration measures at panel points into the equations presented in section 3.3. These results are compared with those measured using a sound intensity probe.

For each of the panels under study (Type A and B), two different output voltages (2 and 5 V_{rms}) were applied from the amplifier that feeds the shaker. At the same time, for each voltage applied, acceleration data were measured at each one of the 108 points on the surface of the panels. Measures were done for two different excitation points (labeled as 69 and 54).

Figure 11 shows the comparison of $L_W(dB)$ curves obtained from the measured accelerations and from the sound intensity probe for both configurations. It can be seen that with the same supplied voltage, panel B radiates higher sound power level than panel A. In addition, it is observed that change in the excitation point does not produce a considerable difference in sound power level pattern, except an increment in the sound power level for both panels.

Specimen	A	B
$E(GN/m^2)$	1.66	0.81
η	0.042	0.019

Table 1: Young's Modulus and Loss factor for specimen A and B.

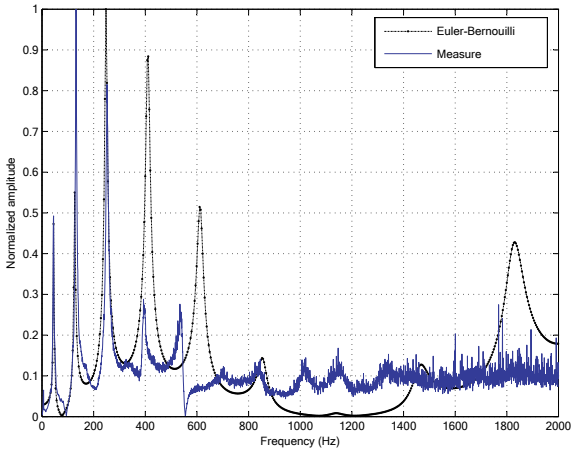

Figure 9: Comparison of theoretical and experimental transfer function for specimen A.

Figure 11 presents the polar directivity plots for different configurations. For different type of panel, the directivities are quite similar and they depend on the frequency of the excitation force.

5 Conclusion

It has been found that a lower value of Young's modulus and damping loss factor produces an increasing of sound power level. At the same time, it appears that the shape of the directivity pattern is not directly affected by the mechanical properties of the material. However, it is observed that the directivity characteristics of the panel are influenced by the frequency of the excitation force. Since the points were chosen close to each other, the directivity is hardly changed. One limitation of the method presented here may be the accuracy of mechanical characteristics of the shaker.

Acknowledgments

This work has been partially supported by BIA2007-68098-C02-01 and Fondecyt 7060073.

References

[1] P. Pintelon, P. Guillaume, S. Vanlanduit, K. De Belder, Y. Rolain, "Identification of Young's modulus from broadband modal analysis exxperiments", *Mech. Syst. and Sig. Proc. 18*, 699-726 (2004)

[2] M.R. Bai, T. Huang, "Development of panel loudspeaker system: Design, evaluation and enhancement", *J. of Acoust. Soc. Am. 109*, 2751-2761 (2001)

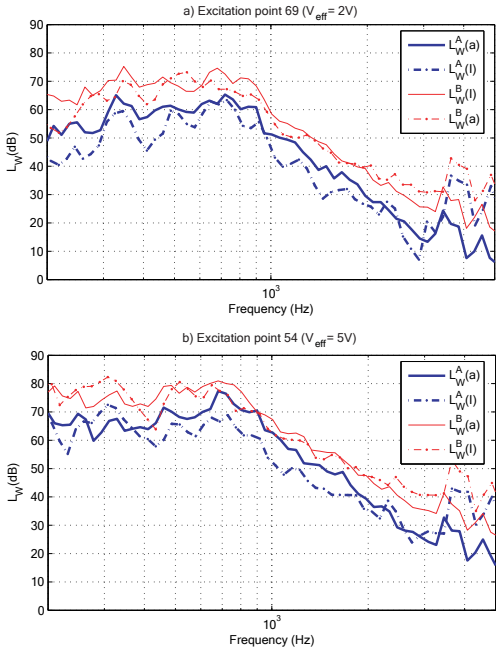

Figure 10: Sound power level radiated from the panels made of material A and B, for two excitation points, using acceleration (a) and sound intensity probe (I).

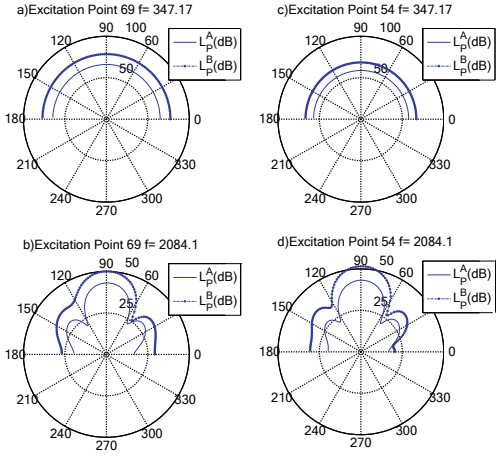

Figure 11: Directivity plots for different panel configurations. The sound pressure level of panel A and B are labeled as L_p^A and L_p^B, respectively.

[3] M.R. Bai, B. Liu, "Determination of optimal exciter deployment for panel speakers using the genetic algorithm", *J. Sound Vib. 269*, 727-743 (2004)

[4] T.-Huo, C.-M. Liaw, "Vibration Acceleration Control of an Inverter-Fed Electrodynamic Shaker", *IEEE/ASME Trans. on Mechs. 4*, 60-70 (1999)

[5] P.M. Morse, K.U. Ingard, *Theoretical Acoustics*, Princeton University Press, Princeton (1968)

[6] D.J. Inman, *Engineering Vibration*, Prentice-Hall, Englewood Cliffs, NJ (1996)

[7] B.H. Tongue, *Principles of Vibration*, Oxford University Press, Oxford (1996)

[8] Designation E 758-98 "Standard Test Method for Measuring Vibration-Damping Properties of Materials", *ASTM International*, PA 19428-2959